Collectivity in the light xenon isotopes: A shell model study

E. Caurier,[1] F. Nowacki,[1] A. Poves,[2,*] and K. Sieja[1]

[1]*IPHC, IN2P3-CNRS et Université Louis Pasteur, F-67037 Strasbourg, France*

[2]*Departamento de Física Teórica e IFT-UAM/CSIC, Universidad Autónoma de Madrid, E-28049 Madrid, Spain*

(Received 20 September 2010; revised manuscript received 3 November 2010; published 9 December 2010)

The lightest xenon isotopes are studied in the shell model framework, within a valence space that comprises all the orbits lying between the magic closures $N = Z = 50$ and $N = Z = 82$. The calculations produce collective deformed structures of triaxial nature that encompass nicely the known experimental data. Predictions are made for the (still unknown) $N = Z$ nucleus ^{108}Xe. The results are interpreted in terms of the competition between the quadrupole correlations enhanced by the pseudo-SU(3) structure of the positive parity orbits and the pairing correlations brought in by the $0h_{11/2}$ orbit. We also have studied the effect of the excitations from the ^{100}Sn core on our predictions. We show that the backbending in this region is due to the alignment of two particles in the $0h_{11/2}$ orbit. In the $N = Z$ case, one neutron and one proton align to $J = 11$ and $T = 0$. In ^{110,112}Xe the alignment begins in the $J = 10$, $T = 1$ channel and it is dominantly of neutron-neutron type. Approaching the band termination the alignment of a neutron-proton pair to $J = 11$ and $T = 0$ takes over. In a more academic mood, we have studied the role of the isovector and isoscalar pairing correlations on the structure on the yrast bands of ^{108,110}Xe and examined the possible existence of isovector and isoscalar pairing condensates in these $N \sim Z$ nuclei.

DOI: 10.1103/PhysRevC.82.064304 PACS number(s): 21.60.Cs, 21.10.Hw, 21.10.Ky, 21.10.Re

I. INTRODUCTION

The lightest xenon isotopes have been recently explored down to ^{110}Xe, only two neutrons away of the still unknown $N = Z$ nucleus ^{108}Xe. In a very demanding experiment carried out at the University of Jyväskylä, using the recoil-decay tagging technique [1], the excitation energies of the lowest members of the yrast band were measured. The experimental spectrum shows appreciable rotational-like features. The authors of this work argue that such a behavior is unexpected and they invoke a large depletion of the doubly magic closure in ^{100}Sn to explain it. However, it is well known that nuclei with six neutrons and four protons on top of a $N = Z$ doubly magic core develop collective features that can be explained microscopically without resorting to extensive core excitations. The same is true, and even more accentuated, for the nuclei with four neutrons and four protons outside the corresponding $N = Z$ cores. Well-documented cases are ^{26}Mg and ^{24}Mg in the sd shell (core of ^{16}O) and ^{50}Cr and ^{48}Cr in the pf shell (core of ^{40}Ca). In both cases the closures correspond to major shells of the harmonic oscillator. The next magic numbers are originated by the spin-orbit interaction, giving rise first to the ^{56}Ni core and to the nuclei ^{66}Ge and ^{64}Ge, which also show collective features, even if less prominent than in the other cases. Indeed, the next $N = Z$ spin-orbit closure is ^{100}Sn, and the replicas of the lower mass isotopes are ^{110}Xe and ^{108}Xe.

For ^{26}Mg and ^{24}Mg, Elliott's SU(3) [2] gives the explanation of the onset of collectivity. Both nuclei are well deformed and triaxial, due to the predominance of the quadrupole-quadrupole part of the effective nuclear interaction, either in the limit of degenerate sd-shell orbits [SU(3) proper] or in the limit of very large spin-orbit splitting [quasi-SU(3) [3]]. ^{48}Cr and ^{50}Cr have became the paradigm of deformed nuclei amenable to a fully microscopic shell model description in the laboratory frame [4–6]. The underlying coupling scheme in this region is quasi-SU(3).

As we shift to the spin-orbit-driven shell closures, the situation varies again. For instance, the quasidegenerate orbits above ^{56}Ni, $1p_{3/2}$, $0f_{5/2}$, and $1p_{1/2}$, form a pseudo-SU(3) sequence [7], with principal quantum number $p = 2$. (We will use p for the principal quantum number of the harmonic oscillator throughout the paper. We decided to do so upon finding that N had already too many uses.) The physical valence space in this region also includes the $0g_{9/2}$ orbit, the down-going intruder of opposite parity, which couples to the pseudo-SU(3) block through the off-diagonal pairing matrix elements. *Mutatis mutandis*, the same physics occurs in the region of very proton-rich nuclei beyond ^{100}Sn. The valence spaces between two spin-orbit closures contain orbits from two major oscillator shells; the intruder orbit from the shell above plus all the orbits from the shell below except the aligned orbit $j = p + 1/2$, which in turn intrudes the next shell below. We use the notation rpl for these spaces; rp indicates what remains of shell p when the aligned orbit $j = p + 1/2$ is removed; l is the orbital angular momentum of the orbit from the shell $p' = p + 1$ with $j' = p' + 1/2$ (in spectroscopic notation). This leads to the spaces $r2f$, $r3g$, $r4h$, $r5i$, etc.

Theoretical work on the proton-rich nuclei above ^{100}Sn has focused mainly on their α and cluster decays [8–10] described by different cluster models. The possible existence of hyperdeformed structures in the region has been addressed in Ref. [11] in the framework of the cranked relativistic mean-field theory. Closer to our work are two very recent articles dealing with spectroscopic issues. In the first one, Nomura *et al.* explore the region using the interacting boson model [12]. In the second one, Delion *et al.* study the role of the

*alfredo.poves@uam.es

proton-neutron correlations in the quasiparticle random phase approximation [13]. Some of their findings will be discussed along with our results.

The plan of the paper is as follows. In Sec. II we describe the framework of the calculations; valence space, effective interaction, etc. We also deal with the group theoretical issues of the pseudo-SU(3) scheme, and advance some of its predictions. In Sec. III we discuss the results for ^{110,112}Xe, comparing them with the experimental results, and we make predictions for ^{108}Xe. Then, we study the influence of the core excitations on the different observables. Finally, we analyze the mechanisms that produce the backbending of the yrast bands of both ^{108}Xe and ^{110}Xe. In Sec. IV we examine in detail some (much debated) aspects of the physics of the $N = Z$ nuclei, including the role of the isovector and isoscalar $L = 0$ pairing components of the interaction. In Sec. V we gather our conclusions.

II. VALENCE SPACE: EFFECTIVE INTERACTION

The valence space is the one comprised between the magic closures $N = Z = 50$ and $N = Z = 82$, $r4h$. This means that we have an inert core of ^{100}Sn. The space contains two doubly magic nuclei, ^{132}Sn and ^{164}Pb.

We use the effective interaction GCN50:82, which is obtained from a realistic G matrix [14] based upon the Bonn-C potential [15]. Taking the G matrix as the starting point, different combinations of two-body matrix elements are fitted to a large set of experimental excitation energies, comprising low-lying states in the following nuclei:

(i) All even-even and even-odd semi-magic nuclei.
(ii) All even-odd Sb isotopes and $N = 81$ isotones.
(iii) Some known odd-odd nuclei around ^{132}Sn.

(In total, about 400 data points from 80 nuclei.) The procedure is similar to the one used in a recent set of papers [16] by Honma *et al.*, which applied the so-called *linear combination* method to derive the GXPF1 interaction for the pf shell. This method allows discriminating among the different linear combinations of the interaction parameters—the single particle energies and the two-body matrix elements—those that can be well determined by the data set considered, from those that are too uncertain to be uniquely determined. In our case, for the final fit, 70 linear combinations were considered as well determined. After several trial runs, it turned out that the solution was not unique. In addition, the modifications brought to the initial realistic interaction were quite large. We solved this problem by modifying the fitting procedure as follows: Instead of varying each one of the 70 well-determined linear combinations at each iteration, we only varied the ten that improved most the interactions (and these were different at each iteration). The fit ended when no other modifications that could significantly improve the interaction could be made with the 70 well-determined linear combinations. We call this procedure "step-by-step" fitting since it successively varies the worst terms of the initial realistic interaction. The final result can be equivalently obtained by successively adding by hand the known relevant parameters of the interaction in the classical fitting method: monopole, pairing, quadrupole, etc. As can be seen in Table I, the modifications of the monopole Hamiltonian are, as usual, the ones that most improve the agreement with the data. Subsequent modifications of the pairing and multipole Hamiltonians bring the root-mean-square (rms) deviation to a very satisfactory value of 110 keV [17].

TABLE I. Evolution of the rms deviation when the different components of the realistic interaction are varied in the fit.

	rms (MeV)
G (bare)	1.350
+monopole	0.250
+pairing	0.180
+multipole	0.110

In the $r4h$ valence space the dimensions grow rapidly, reaching O(10^{10}) in some of the calculations presented here. In spite of this, one can anticipate the kind of results that can be achieved in this model space by taking the limit of pure pseudo-SU(3) symmetry. This requires adopting the $r4$ space with degenerate single particle energies and a pure quadrupole-quadrupole interaction. The quadrupole properties of the Nilsson-like orbits of pseudo-SU(3) in a shell with principal quantum number p' are the same as those of the SU(3) orbits with principal quantum number $p = p' - 1$. The SU(3) orbits with principal quantum number p have intrinsic quadrupole moments given in Ref. [18], $q_0(p, \chi, k) = (2p - 3\chi)b^2$, where χ can take integer values between 0 and p, $k = \pm(\frac{1}{2} \cdots \frac{1}{2} + \chi)$, and b is the harmonic oscillator length parameter. This result is trivially obtained using the Cartesian representation of the SU(3) solutions. The total intrinsic quadrupole moment Q_0 is the sum of the contributions of all the valence protons and neutrons with the corresponding effective charges. In this work we adopt standard effective charges $q_\pi^{\text{eff}} = 1.5q_\pi$ and $q_\nu^{\text{eff}} = 0.5q_\pi$. The orbits are filled orderly, starting from $\chi = 0$ or $\chi = p$, depending on which choice gives the largest total intrinsic quadrupole moment in absolute value. This is true because in this scheme the correlation energy is proportional to Q_0^2.

The four valence protons of the xenons can adopt several degenerate configurations as follows:

$$\begin{aligned}
&\left(\chi = 0, k = \pm\tfrac{1}{2}\right)^2\left(\chi = 1, k = \pm\tfrac{1}{2}\right)^2,\\
&\left(\chi = 0, k = \pm\tfrac{1}{2}\right)^2\left(\chi = 1, k = \pm\tfrac{3}{2}\right)^2, \quad \text{and}\\
&\left(\chi = 0, k = \pm\tfrac{1}{2}\right)^2\left(\chi = 1, k = \pm\tfrac{1}{2}\right),\\
&\left(\chi = 1, k = \pm\tfrac{3}{2}\right),
\end{aligned}$$

leading to $K = 0$ and $K = 2$. Even a small K mixing produces triaxiality, and we should expect it to show up in the experiments and in the realistic calculations.

Moving to the neutron side, the model predicts that the triaxiality should be larger in ^{108}Xe than in ^{110}Xe because of the neutron contribution. In addition, it turns out that for $p = 3$ the contribution to the intrinsic quadrupole moments of

TABLE II. $B(E2)(2^+ \to 0^+)$ for the xenon isotopes (in e^2 fm^4).

$A =$	114	116	118	120	122
p-SU(3)	2100	2540	3040	3200	3240
EXP.	1860(120)	2420(120)	2800(140)	3460(220)	2800(120)

the valence neutrons in excess of six is zero. The predicted values for the light xenon isotopes are: $Q_0(^{108}\text{Xe}) = 210e$ fm^2 and $Q_0(^{110-116}\text{Xe}) = 225e$ fm^2. This corresponds to $B(E2)$ $(2^+ \to 0^+)$ of $870e^2$ fm^4 and $1000e^2$ fm^4, respectively. Therefore, the increase of collectivity that is seen experimentally toward mid-shell, reaching a maximum in ^{120}Xe with 16 valence neutrons cannot be explained in this scheme. To obtain more quadrupole collectivity we need to enlarge the valence space, and the more conservative choice is to include the $1f_{7/2}$ neutron orbit, which is the quasi-SU(3) partner of the $0h_{11/2}$. Assuming that the valence neutrons in excess of six occupy the lowest quasi-SU(3) intrinsic orbits corresponding to $p = 5$, the quadrupole moments will keep increasing up to ^{120}Xe, as demanded by the experimental data.

In Table II, we compare the predictions of this schematic model with the experimental results compiled in Ref. [19]. The agreement is surprisingly good in view of its simplicity. We have made exploratory calculations for ^{112}Xe finding an increase of the $B(E2)$ from $1130e^2$ fm^4 in the pseudo-SU(3) valence space to $1460e^2$ fm^4 in the space corresponding to the proposed pseudo + quasi-SU(3) scenario.

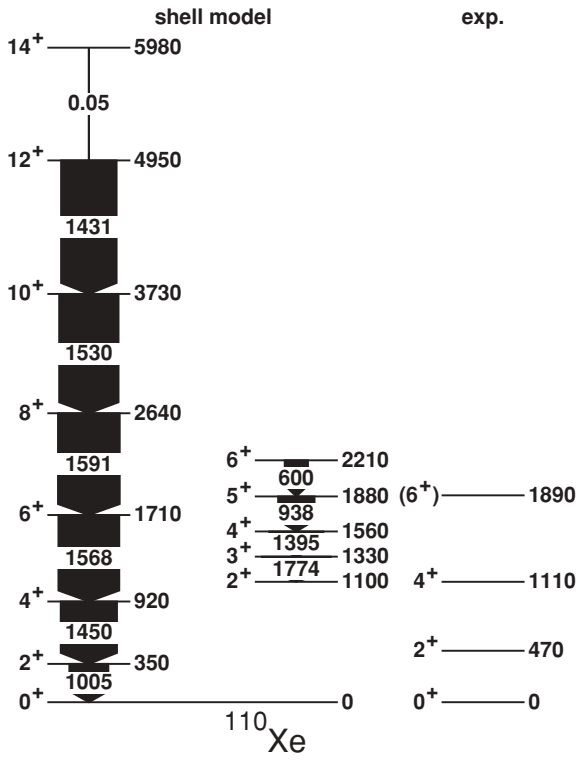

FIG. 1. The energy levels of ^{110}Xe.

III. SPECTROSCOPY OF THE LIGHT XENON ISOTOPES

A. ^{110}Xe

Let us start with the results for ^{110}Xe. The calculated energy levels are shown in Fig. 1, in comparison with the experimental results from Ref. [1]. The agreement is quite satisfactory even if the theoretical calculation predict a moment of inertia slightly larger than the experimental one. We have checked that it is possible to obtain perfect agreement for the excitation energies, without changing the quadrupole properties of the band, but by just increasing ∼20% the isovector pairing channel of the effective interaction. Nevertheless, this residual discrepancy does not justify making modifications in the effective interaction GCN50:82, which was designed to give good spectroscopy in the full $r4h$ valence space. Notice that the rotational features of the shell model calculation persist until the backbending that occurs at $J = 14$, due to the alignment of two neutrons to $J = 10$ in the $0h_{11/2}$ orbit. In addition, the calculation produces a γ band, which we will analyze below.

In Table III, we collect the quadrupole properties of the yrast band, $B(E2)$'s, and spectroscopic quadrupole moments Q_{spec}. We derive the intrinsic quadrupole moments Q_0 either from the $B(E2)$'s or from the spectroscopic ones using the following well-known relations:

$$Q_0 = \frac{(J+1)(2J+3)}{3K^2 - J(J+1)} Q_{\text{spec}}(J), \quad K \neq 1, \tag{1}$$

and

$$[B(E2), (J \to J-2)] = \tfrac{5}{16} e^2 |\langle JK20|J-2, K\rangle|^2 Q_0^2, \tag{2}$$

for $K \neq \frac{1}{2}, 1$. We conclude that the results are compatible with a deformed intrinsic state with nearly constant quadrupole moment $Q_0 = 200e$ fm^2, corresponding to $\beta = 0.16$, not far

TABLE III. Properties of the yrast band of ^{110}Xe [energies in MeV, Q's in e fm^2, and $B(E2)$'s in e^2 fm^4].

J	E^*	E_γ	$B(E2)$	Q_{spec}	Q_0 from $B(E2)$	Q_0 from Q_{spec}	β
2^+	0.35	0.35	1005	−62	225	217	0.17
4^+	0.92	0.57	1450	−78	226	215	0.17
6^+	1.71	0.79	1568	−83	224	208	0.17
8^+	2.64	0.93	1591	−87	220	207	0.17
10^+	3.73	1.09	1530	−86	213	198	0.17
12^+	4.95	1.22	1431	−85	204	191	0.16
14^+	5.98	1.03	0.05	−126			
16^+	6.63	0.65	111	−125			
18^+	7.51	0.88	1184	−130			
20^+	8.51	1.00	1043	−134			

TABLE IV. Properties of the γ band of ^{110}Xe [energies in MeV, Q's in e fm^2, and $B(E2)$'s in e^2 fm^4].

J	E^*	E_γ	$B(E2)$	$Q_{\rm spec}$	Q_0 from $B(E2)$	Q_0 from $Q_{\rm spec}$	β
2_2^+	1.10			+61		214	0.17
3^+	1.33	0.23	1774	−1.3			
4_2^+	1.56	0.23	1395	−38	219	261	0.18
5^+	1.88	0.32	938	−54	217	234	0.17
6_2^+	2.21	0.33	600	−74	209	259	0.18

from the expectations of the pseudo-SU(3) model. Beyond $J = 12$, the alignment regime takes over (as we shall analyze in detail in the next sections), and the rotation is no longer collective.

We can now come back to the γ band. Besides the characteristic sequence of energy levels shown in Fig. 1, the quadrupole properties of the band, gathered in Table IV, strongly suggest that the γ band of ^{110}Xe has $K = 2$. In the first place, the intrinsic quadrupole moment, extracted from the spectroscopic quadrupole moments or from the $B(E2)$'s, assuming $K = 2$, is fairly constant and very close to that of the yrast band. In addition, $Q(2_\gamma^+) = -Q(2_y^+)$ and $Q(3^+) \approx 0$, as it should be if the γ band were $K = 2$.

The question now is whether ^{110}Xe is a triaxial nucleus or not. For that, a certain amount of K mixing is required. In fact, in the limit of pure pseudo-SU(3) symmetry the mixing is zero and this would not be the case. In some models [20], the amount of triaxiality, γ, is derived from the ratio:

$$\frac{[B(E2), (2_\gamma^+ \to 2_y^+)]}{[B(E2), (2_\gamma^+ \to 0_y^+)]}. \tag{3}$$

With the shell model values for the $B(E2)$'s of these transitions we extract a value of $\gamma = 20^{\rm o}$.

The valence space $r4h$ contains a pseudo-SU(3) triplet plus the intruder orbit $0h_{11/2}$. When we remove the intruder orbit from the space, the moment of inertia of the nucleus almost doubles, the backbending is suppressed, the triaxiality is reduced to $\gamma = 12^{\rm o}$; and the magnetic moments become fully consistent with the rotational model up to $J = 20$. The changes in the $E2$ transition probabilities and quadrupole moments below the backbending region are negligible. This is in full agreement with what we had found in other regions [21]; the fact that when the rotational regime is established, the main effect of the pairing interaction is to reduce the moment of inertia. The disappearance of the backbending when the $0h_{11/2}$ orbit is not present seems to be particular for this region, because (as we have already mentioned) the backbending is due to the alignment of two neutrons in the intruder orbit, which may not be a general rule.

B. ^{112}Xe

The shell model description of this isotope is a real challenge because the dimension of the basis in the full space calculation (number of $M = 0$ Slater determinants) is $\sim 10^{10}$ (exactly 932 475 1339). The results are gathered in Table V and compared with the available experimental data [22]. For the lowest part of the yrast band they closely resemble those of ^{110}Xe and the agreement with the experimental excitation energies is even better. Nevertheless, when entering in the backbending region, which is predicted by the calculation at the right spin ($J = 10$), the accord deteriorates. As we have discussed in the previous sections, this can be a manifestation of the limitations of our valence space for the description of the heavier xenon isotopes. The backbending corresponds with the alignment of two neutrons in the $0h_{11/2}$ orbit as in the lighter isotope ^{110}Xe. This change of structure is clearly seen in the drastic reduction of the $B(E2)$ of the $10^+ \to 8^+$ transition, which is simultaneous with an increase of the spectroscopic quadrupole moment of the 10^+ state. In both ^{110}Xe and ^{112}Xe, the shell model deformation parameters β are in good accord with the ones obtained in Ref. [12]. On the contrary, the interacting boson model solutions peak at $\gamma = 0$ in contradistinction with our results. Nevertheless, as the IBM projected energy surfaces are rather flat in the γ direction, triaxiality may be restored after configuration mixing.

TABLE V. Properties of the yrast band of ^{112}Xe [energies in MeV, Q's in e fm^2, and $B(E2)$'s in e^2 fm^4].

J	E^*	$E_{\rm exp}$	$B(E2)$	$Q_{\rm spec}$	Q_0 from $B(E2)$	Q_0 from $Q_{\rm spec}$	β
2^+	0.38	0.46	1063	−62	217	231	0.17
4^+	1.00	1.12	1560	−75	206	236	0.17
6^+	1.82	1.91	1727	−76	190	236	0.17
8^+	2.79	2.78	1783	−74	176	232	0.17
10^+	3.72	3.55	600	−97			
12^+	4.20	4.47	1471	−118			

C. ^{108}Xe

The $N = Z$ isotope of Xenon has not been experimentally studied yet. The shell model predictions for the yrast band are collected in Table VI. The results at low spin very much resemble the ones obtained for the heavier isotopes,

TABLE VI. Properties of the yrast band of ^{108}Xe [energies in MeV, Q's in e fm^2, and $B(E2)$'s in e^2 fm^4].

J	E^*	E_γ	$B(E2)$	$Q_{\rm spec}$	Q_0 from $B(E2)$	Q_0 from $Q_{\rm spec}$	β
2^+	0.41	0.41	888	−57	200	211	0.16
4^+	1.03	0.62	1285	−71	195	210	0.16
6^+	1.89	0.86	1345	−65	163	208	0.16
8^+	2.90	1.01	1404	−64	154	206	0.16
10^+	4.03	1.13	1334	−67	160	198	0.15
12^+	5.37	1.34	1129	−71	175	182	0.15
14^+	6.69	1.32	990	−79	176	168	0.14
16^+	7.75	1.06	0.1	−137			
18^+	8.34	0.59	830	−140			
20^+	9.24	0.90	753	−143			

TABLE VII. Properties of the γ band of ^{108}Xe [energies in MeV, Q's in e fm^2, and $B(E2)$'s in e^2 fm^2].

J	E^*	E_γ	$B(E2)$	$Q_{\rm spec}$	Q_0 from $Q_{\rm spec}$	β
2_2^+	1.03			+59	196	0.16
3^+	1.28	0.25	1624	−1.3		
4_2^+	1.51	0.23	1090	−38	265	0.18
5^+	1.84	0.33	882	−51	220	0.17
6_2^+	2.25	0.41	372	−83	290	0.19

even if the the quadrupole collectivity is slightly smaller. The backbending occurs at $J = 16$ and it is preceded by an upbending at $J = 14$, while in ^{110}Xe the backbending occurs sharply at $J = 14$. We shall discuss this issue in the next section. As predicted by the pseudo-SU(3) model, ^{108}Xe also exhibits a γ band whose properties are listed in Table VII. Notice that in spite of some small irregularities both the yrast and the γ band share a common intrinsic state whose quadrupole moment is very close to the pseudo-SU(3) number. Using Eq. (3) we can deduce a value of $\gamma = 24^o$, indicating the triaxial nature of this nucleus. This value of γ is larger than the one obtained for ^{110}Xe, again in good accord with the model predictions.

D. The effect of the excitations of the ^{100}Sn core

Above, we introduced the question about the stiffness of the ^{100}Sn core and the eventual need of a soft core in order to understand the collective aspects found in very proton-rich xenon isotopes. We have argued *in extenso* that collectivity can be obtained without any opening of the doubly magic ^{100}Sn core. However, such a thing does not exist in nature as a perfectly closed core. The dimensions of the basis make it impossible to perform calculations adding the $0g_{9/2}$ orbit to the $r4h$ valence space. Thus, we have proceeded as follows: In the first place, we have repeated the calculations in the $r4$ space (i.e., removing the $0h_{11/2}$ orbit). The quadrupole properties of the low-lying states—the ones we are after—remain unchanged in all cases. For the lower part of the yrast band, the effect of this removal is just an increase of the moments of inertia by a factor of 2. Correspondingly, the spectra are much more compressed. In the next set of calculations we allow $1p$-$1h$ and $2p$-$2h$ excitations from the $0g_{9/2}$ orbit into the $r4$ space. Even in this case the dimensions are huge (5×10^9 for the $2p$-$2h$ calculation in ^{110}Xe), and in fact, the $2p$-$2h$ calculation for ^{112}Xe is out of reach. In these calculations, ^{100}Sn is still a very good doubly closed shell. At the $1p$-$1h$ level only 0.25 particles (out of 20) are promoted to the $r4$ orbits. At the $2p$-$2h$ level 0.5 particles are promoted. In spite of the small size of the vacancy, its effect in the $E2$ properties is not negligible at all. The $1p$-$1h$ excitations are the ones that are more efficient in the building up of the quadrupole collectivity, leading to increases of the intrinsic quadrupole moments of 15%, 17%, and 20% for ^{108}Xe, ^{110}Xe, and ^{112}Xe, respectively. Adding the $2p$-$2h$ excitations does not change these numbers a lot; they rise to 19% and 21% for ^{108}Xe and ^{110}Xe, respectively. Notice that these percentages have to be doubled to get the effect on the transition probabilities.

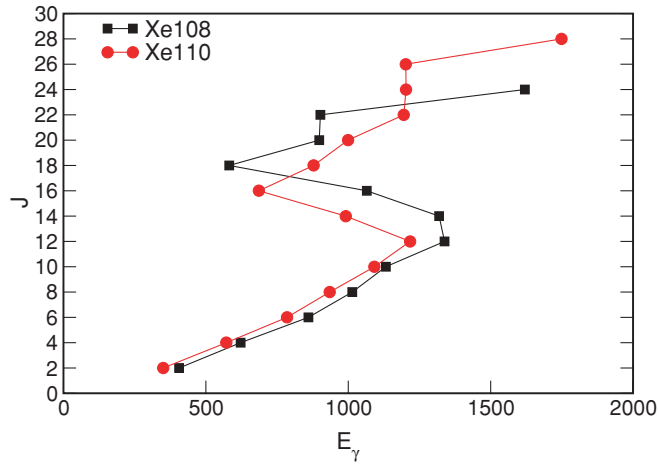

FIG. 2. (Color online) Backbending plot of the theoretical yrast bands of ^{108}Xe and ^{110}Xe.

E. Backbending and alignment

We have represented the energies of the $E2$ γ cascade along the yrast bands of ^{108}Xe and ^{110}Xe in the form of a backbending plot in Fig. 2. We can observe a very similar (collective) behavior up to the backbending that occurs at $J = 14$ in both cases. The differences are related to the alignment mechanisms that produce it, whose nature we will explore now. In order to do so, we have constructed operators that count the number of $0h_{11/2}$ pairs coupled to $J = 11, T = 0$ and to $J = 10, T = 1$. In the first case, the particles that align must be one neutron and one proton, while in the second mode they can be two neutrons or two protons as well. Let us start with ^{108}Xe.

The number of $J = 11, T = 0$ neutron-proton pairs along the yrast band is shown in Fig. 3. We observe a sudden

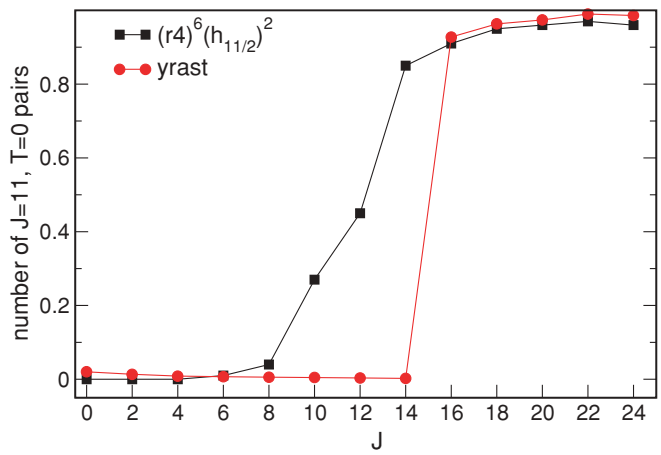

FIG. 3. (Color online) The number of $J = 11$, $T = 0$ pairs in the yrast band of ^{108}Xe and for the yrast states of the configuration $(r4)^6(h_{11/2})^2$.

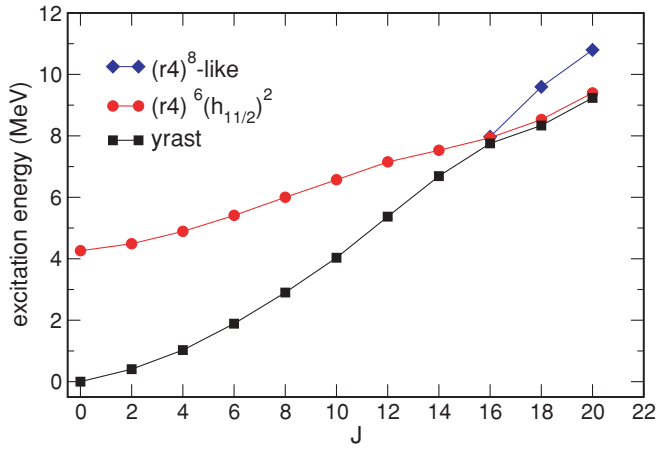

FIG. 4. (Color online) The yrast band of ^{108}Xe. Also plotted are the yrast states of the configuration $(r4)^6(h_{11/2})^2$ (circles) and the lowest $(r4)^8$-like states beyond $J = 16$ (lozenges) to illustrate the origin of the backbending.

transition from zero aligned pairs up to $J = 14$, to nearly one fully aligned pair at $J = 16$. From there, up to the band termination, the number of aligned pairs slowly approaches 1. This reflects in the backbending in a subtle way. As we can see, the real backbending in this case is preceded by an upbending, which does not involve alignment but is probably due to the mixing associated to the band crossing. In Fig. 3 we have plotted the yrast band of the configuration that has two particles blocked in the $0h_{11/2}$ orbit. Here, the alignment is much smoother. Notice that only when this configuration is fully aligned does it become the physical yrast band.

This is better seen in Fig. 4, where the mechanism of the band crossing is evident. At low spin the yrast band is dominated by the $(r4)^8$ configurations, with the $(r4)^6(h_{11/2})^2$ ones lying at about 4 MeV. The crossing happens at $J = 16$, producing local distortions in the backbending plot. We have been able to locate the states belonging to the $(r4)^8$ yrast band beyond the crossing point. Once the crossing has taken place, the backbending disappears.

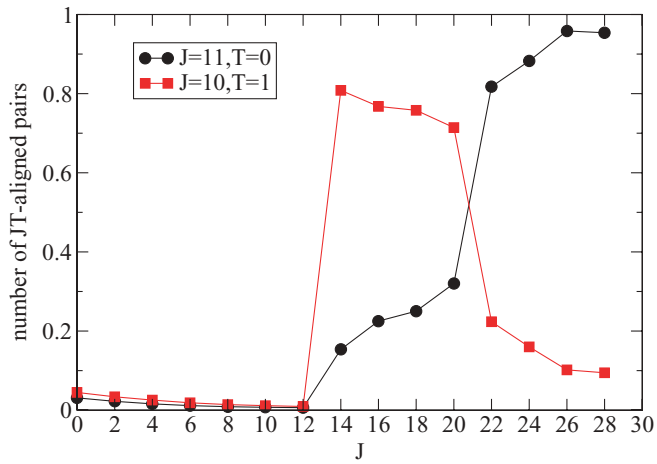

FIG. 5. (Color online) The number of $J = 10, T = 1$ and $J = 11$, $T = 0$ pairs in the yrast band of ^{110}Xe.

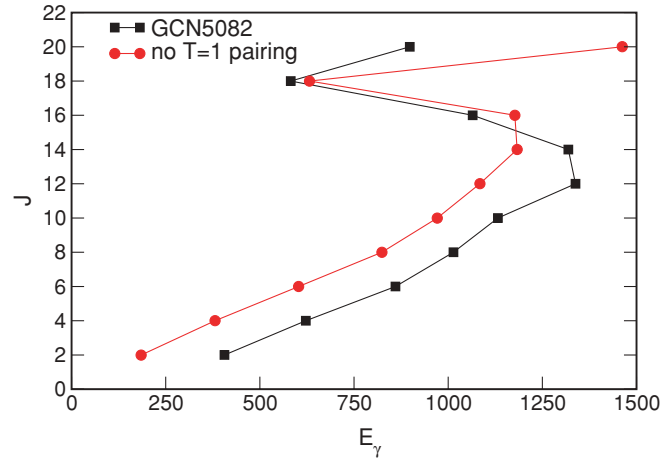

FIG. 6. (Color online) Backbending plot of the yrast band of ^{108}Xe. Results with the GCN5082 interaction before (squares) and after (circles) removing the isovector $J = 0$ pairing.

The situation is quite different in the case of the $N \neq Z$ nucleus ^{110}Xe, as can be gathered from Fig. 5. Here, the backbending occurs abruptly at $J = 14$ and corresponds to the alignment of (mostly) two neutrons to $J = 10, T = 1$. Beyond $J = 16$, the yrast line becomes parallel to the low energy one, as if the angular momentum put in the system were again of a collective nature. At $J = 22$, the isovector alignment is depressed and the isoscalar one takes over until the band termination, producing new irregularities in the backbending plot.

IV. THE ROLE OF THE ISOSCALAR AND ISOVECTOR PAIRING

Quite some time ago, there was an increase of interest in the question of the pairing modes near $N = Z$ as more and more experimental data accumulated about this class of nuclei. Among the topics of interest were the Wigner energy and the possibility of finding manifestations of an isoscalar pairing condensate (deuteron-like) in the yrast bands of these proton-

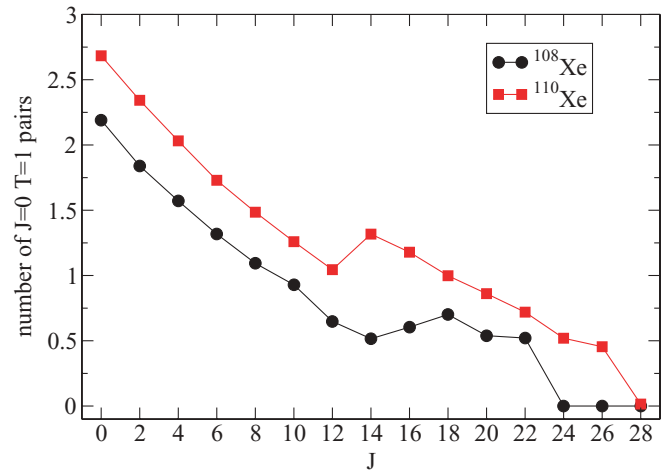

FIG. 7. (Color online) The number of $J = 0$, $T = 1$ pairs in the yrast bands of ^{108}Xe and ^{110}Xe.

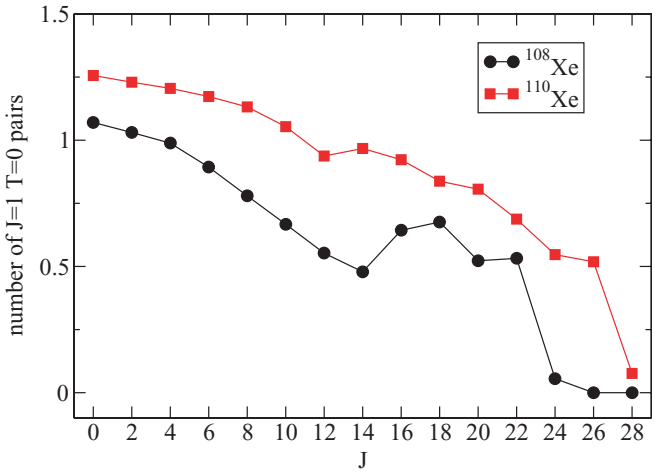

FIG. 8. (Color online) The number of $J = 1$, $T = 0$ pairs in the yrast bands of ^{108}Xe and ^{110}Xe.

rich nuclei in the form of delayed alignments, etc. [23,24]. It was realized relatively soon that these effect were bound to be elusive, because, in normal circumstances, spin-orbit splitting strongly hinders the deuteron-like condensation [21]. Recent studies of the β decay of ^{62}Ge, where super-allowed β transitions due to the existence of the $T = 0$ collective 1^+ state were predicted [25], have ruled out such a possibility as well.

On the contrary, the effect of the isovector pairing channel in the rotational properties of the $N \sim Z$ is well understood. It is directly linked to the moment of inertia of the band, and does not affect appreciably its electromagnetic decay properties. We have verified this for the light xenon isotopes. In Fig. 6, we compare the energies of the γ cascades along the yrast band for ^{108}Xe using the effective interaction GCN5082 on one side and, on the other side, this same interaction after removal of an schematic isovector pairing Hamiltonian whose coupling strength is obtained as in Ref. [26]. Below the backbending, the effect is just an increase of the moment of inertia by a factor of 2. As expected, the $E2$ properties do not change. The backbending is delayed by two units of angular momentum. Removing a schematic $T = 0$ pairing produces similar qualitative features that are quantitatively irrelevant. Therefore, our results refute the claim of Ref. [13] about the reduction of collectivity due to the neutron-proton pairing interaction.

To verify the possibility of existence of pair condensates in the ground states of Xenon isotopes, we have also constructed pair counting operators and have computed their expectation values along their yrast bands. The results for the isovector pairs are plotted in Fig. 7. A fully condensed state should have nearly four pairs for ^{108}Xe and five pairs in ^{110}Xe. What we find for the ground states, which is consistent in both cases, amounts to one- half of the value expected for the condensate; indeed, quite an important pairing contribution. As the angular momentum increases, the pair content decreases linearly, reaching negligible values at the backbending. The pattern in this region is simpler in ^{108}Xe than in ^{108}Xe due to the different alignment mechanisms in both isotopes, which we have discussed already.

The results for the isoscalar pairs are plotted in Fig. 8. In the limit of an isovector condensate, typically, we should expect four pairs, and we can see that we are far from that. In addition, the *a priori* more favorable case, $N = Z$, is depressed with respect to the $N \neq Z$. All in all, there seems to be no indications of any structural effect due to the isoscalar pairing channel.

V. CONCLUSIONS

We have carried out large-scale shell model calculations for the lighter xenon isotopes in the valence space $r4h$ that encompasses all the orbits between the magic numbers 50 and 82. We obtained collective behaviors of triaxial nature and reproduced the experimental results without resorting to large openings of the ^{100}Sn core. We propose a mechanism that can explain the very large values of the intrinsic quadrupole moments of the xenon isotopes at the midneutron shell based on variants of the SU(3) symmetry. We have shown that the backbending in ^{108}Xe is produced by the alignment of a neutron-proton pair in the $0h_{11/2}$ orbit to the maximum allowed spin $J = 11$. In ^{110}Xe, it is a two-step process: first, a pair of neutrons align to $J = 10$ and, second, the neutron-proton alignment takes over. Finally, we have studied the pair content of the yrast states. Isovector $J = 0$ pairs have a large presence in the lowest states of the yrast bands of ^{108}Xe and ^{110}Xe. On the contrary, the deuteron-like $J = 1$ isoscalar pairs have a negligible presence in these nuclei.

ACKNOWLEDGMENTS

This work is partly supported by a grant from the Spanish Ministry of Education and Science (FPA2009-13377), by the IN2P3(France)-CICyT(Spain) collaboration agreements, by the Spanish Consolider-Ingenio 2010 Program CPAN (CSD2007-00042), and by the Comunidad de Madrid (Spain), project HEPHACOS S2009/ESP-1473.

[1] M. Sandzelius *et al.*, Phys. Rev. Lett. **99**, 022501 (2007).
[2] J. P. Elliott, Proc. R. Soc. London Ser. A **245**, 128 (1956).
[3] A. P. Zuker, J. Retamosa, A. Poves, and E. Caurier, Phys. Rev. C **52**, R1741 (1995).
[4] E. Caurier, J. L. Egido, G. Martínez-Pinedo, A. Poves, J. Retamosa, L. M. Robledo, and A. P. Zuker, Phys. Rev. Lett. **75**, 2466 (1995).
[5] G. Martínez-Pinedo, A. Poves, L. M. Robledo, E. Caurier, F. Nowacki, J. Retamosa, and A. P. Zuker, Phys. Rev. C **54**, R2150 (1996).
[6] S. M. Lenzi *et al.*, Z. Phys. A **354**, 117 (1996).
[7] K. T. Hetch and A. Adler, Nucl. Phys. A **137**, 129 (1969).
[8] C. Xu and Z. Ren, Phys. Rev. C **74**, 037302 (2006).

[9] C. Qi, F. R. Xu, R. J. Liotta, R. Wyss, M. Y. Zhang, C. Asawatangtrakuldee, and D. Hu, Phys. Rev. C **80**, 044326 (2009).
[10] D. Ni and Z. Ren, Nucl. Phys. A **834**, 370c (2010).
[11] A. V. Afanasjev and H. Abusara, Phys. Rev. C **78**, 014315 (2008).
[12] K. Nomura, N. Shimizu, and T. Otsuka, Phys. Rev. C **81**, 044307 (2010).
[13] D. S. Delion, R. Wyss, R. J. Liotta, Bo Cederwall, A. Johnson, and M. Sandzelius, Phys. Rev. C **82**, 024307 (2010).
[14] M. Hjort-Jensen, T. T. S. Kuo, and E. Osnes, Phys. Rep. **261**, 126 (1995).
[15] R. Machleidt, F. Sammarruca, and Y. Song, Phys. Rev. C **53**, R1483 (1996).
[16] M. Honma, T. Otsuka, B. A. Brown, and T. Mizusaki, Phys. Rev. C **65**, 061301(R) (2002); **69**, 034335 (2004).
[17] A. Gniady, E. Caurier, and F. Nowacki (to be submitted).
[18] E. Caurier, G. Martínez-Pinedo, F. Nowacki, A. Poves, and A. P. Zuker, Rev. Mod. Phys. **77**, 427 (2005).
[19] Brookhaven National Nuclear Data Center (NNDC) [http://www.nndc.bnl.gov].
[20] A. S. Davidov and G. F. Filipov, Nucl. Phys. **8**, 237 (1958).
[21] A. Poves and G. Martínez-Pinedo, Phys. Lett. B **430**, 203 (1998).
[22] J. F. Smith *et al.*, Phys. Lett. B **523**, 13 (2001).
[23] W. Satula, D. J. Dean, J. Gary, and W. Nazarevicz, Phys. Lett. B **407**, 103 (1997).
[24] J. Dobes and S. Pittel, Phys. Rev. C **57**, 688 (1998).
[25] I. Peterman, G. Martínez-Pinedo, K. Langanke, and E. Caurier, Eur. Phys. J. A **34**, 319 (2007).
[26] M. Dufour and A. P. Zuker, Phys. Rev. C **54**, 1641 (1996).